Catalysis Letters
https://doi.org/10.1007/s10562-017-2272-5

Silver Nanoparticles Engineered β-Cyclodextrin/γ-Fe_2O_3@ Hydroxyapatite Composite: Efficient, Green and Magnetically Retrievable Nanocatalyst for the Aqueous Reduction of Nitroarenes

Maedeh Azaroon[1] · **Ali Reza Kiasat**[1,2]

Received: 19 October 2017 / Accepted: 3 December 2017

Abstract

Ag nanoparticles incorporated β-cyclodextrin conjugated magnetic hydroxyapatite, γ-Fe_2O_3@HAp-CD.Ag was conveniently synthesized via the grafting of β-cyclodextrin moieties on the hydroxyapatite surface, followed by reacting of the nanocomposite, γ-Fe_2O_3, with silver nitrate and then its reduction with sodium borohydride. The cavity of β-cyclodextrin units as host material can stabilize the Ag nanoparticles (particles size: 12–14 nm) effectively and prevent their aggregation and separation from the surface. The nanocomposite obtained appears to have an organized structure, with a magnetic γ-Fe_2O_3 core surrounded by a layer-structured coating shell. The structure and composition of the nanocomposite were confirmed by FT-IR, FE-SEM, TEM, TGA, XRD, EDS, BET, and VSM. This catalytic system selectively reduces the nitro group even in the presence of other sensitive functional groups in good to excellent yields (85–98%).The organometallic nanocatalyst was easily removed from solution using an external magnet and was successfully examined for five runs, with a slight loss of catalytic activity.

Graphical Abstract

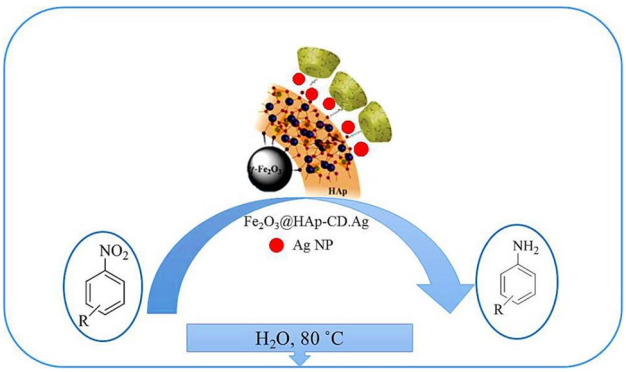

Keywords γ-Fe_2O_3@HAp-CD.Ag · Heterogeneous nanocatalyst · Reduction of nitroarenes · Silver nanoparticle · Green chemistry

1 Introduction

Today, as we know, all governments and research centers around the world recognize that green chemistry leads to a cleaner and sustainable earth, and is also very beneficial in terms of economic and social effects. These benefits encourage industries to implement environmentally friendly

Electronic supplementary material The online version of this article (https://doi.org/10.1007/s10562-017-2272-5) contains supplementary material, which is available to authorized users.

✉ Maedeh Azaroon
m-azaroon@phdstu.scu.ac.ir

Extended author information available on the last page of the article

Published online: 18 December 2017

technologies. The largest amount of "auxiliary waste" in most chemical processes is associated with solvent and non-recyclable homogenous catalyst usage; accordingly, a part of green chemistry connects to solve this challenge. Industries have begun to use green chemistry and its applications such as new heterogeneous catalysts and waste prevention to use less toxic solvents and reagents [1–7].

In the last years, inorganic supports, such as hydroxyapatite (HAp) have attracted many scientists [8–10]. It is the mesoporous solid support with high surface area, availability, environment-friendly nature, and an ability to design new functionalized material which can make hydroxyapatite-encapsulated magnetic nanocrystallites an excellent support for the preparation of heterogeneous catalysts in organic chemistry [11–15].

The unique structure and properties of cyclodextrins (CDs) have made them a popular choice for a wide range of applications over the past few decades. They play major roles in many disciplines such as supramolecular chemistry, catalysis and biomedicine [16–18]. CDs have truncated cone-like three-dimensional structures with hydrophilic exteriors and hydrophobic cavities that endow them with a special ability to accommodate many organic compounds by inclusion complexation because they can be linked both non-covalently and covalently [19, 20].

In recent years, cyclodextrins have increasingly been used in the preparation of metal nanoparticles such as palladium, platinum and silver [21–23]. In addition, supported transition-metal catalysis having high activity and selectivity are currently attracting great interest in the development of industrial processes, in particular in fine chemical production. Nitroarene compounds have different hazardous effect to the environment and heath. these compounds have been introduced into the environment by human activities such as dyeing industries, plastics and agriculture, etc. The catalytic reduction of nitroarene compounds in sustainable method with green solvent like water is one of the most important methods for the decontamination of nitroarene compounds [24–41]. In this context, a considerable number of studies on the catalytic reactions of silver NPs have been conducted, such as alcohol dehydrogenation, Diels–Alder cycloadditions, and reduction of aromatic compounds [42–54]. However, during a reaction, the highly active surface atoms destabilize the NPs. To overcome this problem, Ag NPs have been immobilized onto mesoporous inorganic supports to increase its stability [55–60].

By considering all the above-mentioned points and in the course of our investigations into the development of novel porous inorganic–organic hybrid heterogeneous nanocatalysts in organic transformation, the aim of this presented work is to highlight the synergistic effects of the combined properties of highly mesoporous surface of magnetic hydroxyapatite, and cyclodextrin cavity, in the trapping and stabilizing of the Ag nanoparticles in order to synthesize high efficient and a reusable nanocatalyst for reduction of nitroarenes to the corresponding aromatic amines by using $NaBH_4$ as reducing agent in water.

2 Experimental

2.1 General

Iron (II) chloride tetrahydrate (99%), iron (III) chloride hexahydrate (98%), β-cyclodextrin and other chemicals were purchased from Fluka and Merck companies and used without further purification. Products were characterized by comparison of their physical and spectral data with those reported in the literatures.

The surface area and pore size distribution of the support was measured by the nitrogen adsorption–desorption method (Belsorp mini II). All the samples were degassed at 120 °C during 2 h before nitrogen adsorption measurements. FT-IR (Fourier transform infrared) spectra were recorded on a Perkin-Elmer (IL74XB3GV5) spectrometer. NMR spectra were recorded in $CDCl_3$ on a Bruker Advance DPX 400 MHz instrument spectrometer using TMS as internal standard. X-ray diffraction (XRD) patterns of catalyst were taken on Philips X-ray diffraction model Research (PANalytical company) with a wavelength $\lambda = 1.54056$ A˚, the diffraction angles (2θ) were set between 10° and 80°. The field emission scanning electron micrograph (FE-SEM) was obtained by FE-SEM instrumentation (MIRA3TESCAN-XMU). An Analytik Jena (Germany) flame AAS instrument was used for determination of Ag, Energy-dispersive X-ray spectroscopy (EDX) analysis was obtained by MIRA3TESCAN-XMU instrument. Transmission electron microscope (TEM) images were obtained using Zeiss – EM10C −80 kV instrument. The TGA curve was recorded on a PC Luxx 409 at heating rates of 10 °C min^{-1}. For magnetization measurement, a vibrating sample magnetometer (VSM) was used at room temperature (Meghnatis Daghigh Kavir Co., Kashan, Iran).

2.2 Preparation of Ag Nanoparticles Incorporated Mesoporous Magnetite–Hydroxyapatite, γ-Fe_2O_3@HAp-CD.Ag

2.2.1 Preparation of Aminopropyl Conjugated Mesoporous Magnetite–Hydroxyapatite, Fe_2O_3@HAp-NH_2

First, the mixture of $FeCl_2{\cdot}4H_2O$ (0.37 g, 1.85 mmol) and $FeCl_3{\cdot}6H_2O$ (1 g, 3.7 mmol) were dissolved in deionized water (30 mL) under Ar atmosphere at room temperature and the resulting solution was added to a 25 wt% NH_4OH solution (10 mL) with vigorous mechanical stirring. A

black precipitate of Fe_3O_4 was produced instantly. In order to obtain small and uniform Fe_3O_4 particles, the drop rate of NH_4OH was controlled precisely by a constant dropper and the drop rate was 1 mL min^{-1}. After 15 min, 100 mL of $Ca(NO_3)_2{\cdot}4H_2O$ (33.7 mmol, 0.5 M) and $(NH_4)_2HPO_4$ (20 mmol, 3.0 M) solutions adjusted to pH 11 were added drop-wise to the obtained precipitate over 30 min with mechanical stirring. The resulting milky solution was heated to 90 °C. After 2 h, the mixture was cooled to room temperature and aged overnight. The dark brown precipitate formed was filtered, washed repeatedly with deionized water until the water was neutral, and then air-dried under vacuum at room temperature. The synthesized sample was calcined at 300 °C for 3 h, giving a reddish-brown powder, Fe_2O_3@HAp.

Then for the linkage of aminopropyl unit to the surface of the obtained support, Fe_2O_3@HAp (1 g) were dispersed in anhydrous toluene (50 mL), with ultrasonication for 15 min and 3-aminopropyltrimethoxysilane (10 mmol) was added. The mixture was heated under reflux for 24 h under Argon protection. The suspended substance was collected by a magnet and rinsed 3 times with ethanol and distilled water,

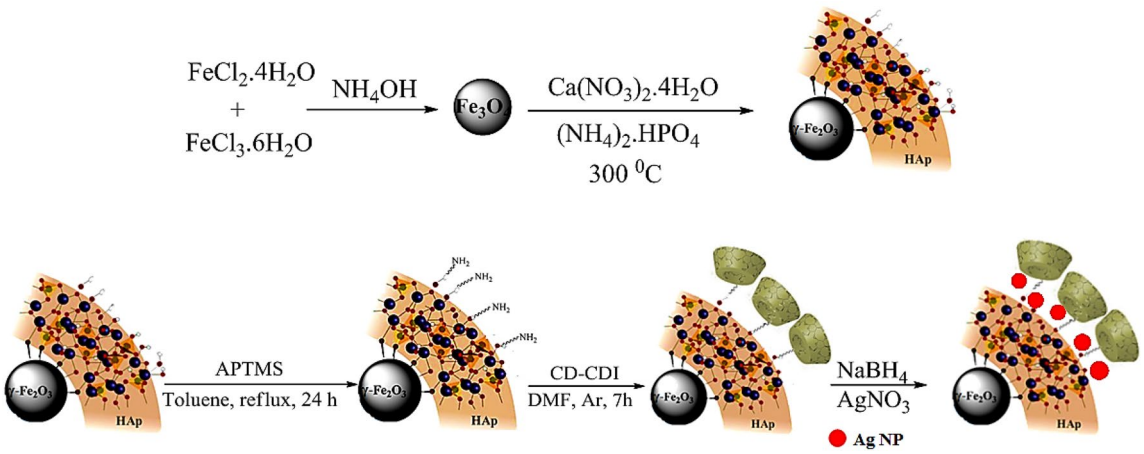

Scheme 1 Synthetic route for γ-Fe_2O_3@HAp-CD.Ag nanocomposite preparation

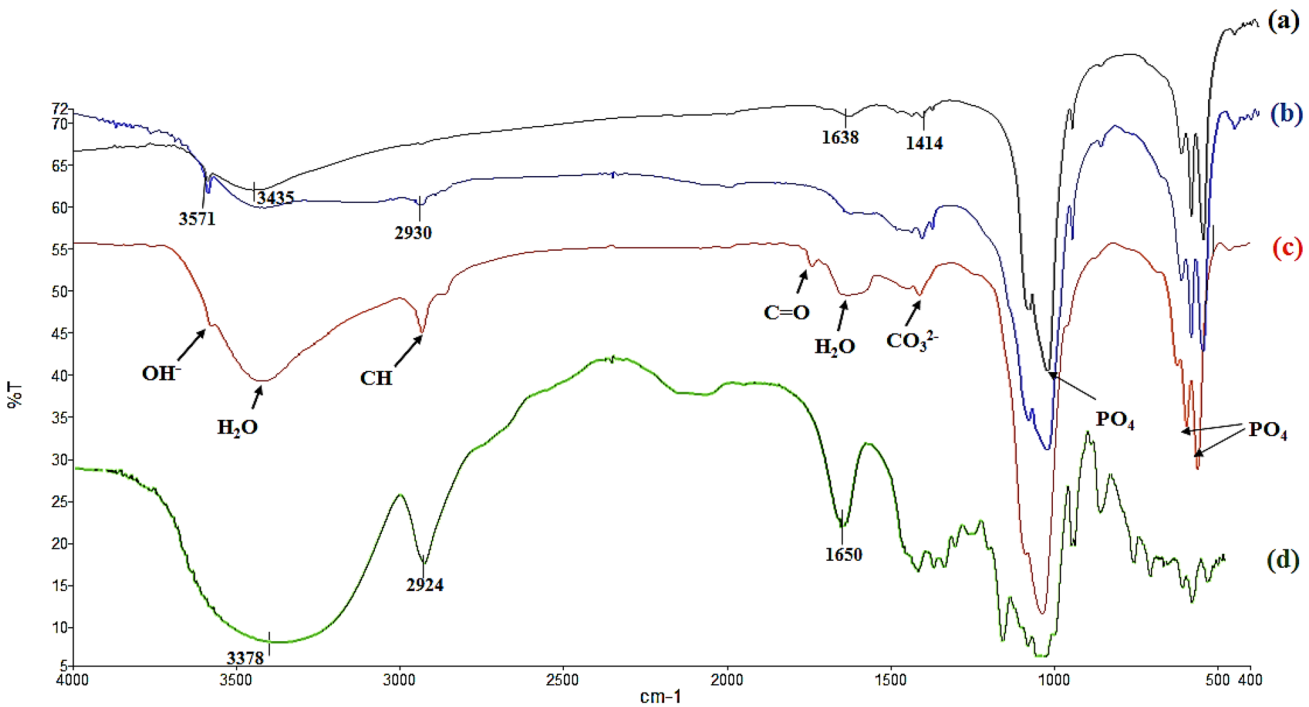

Fig. 1 The FT-IR spectra of *a* Fe_2O_3@HAp, *b* Fe_2O_3@HAp-NH_2, *c* Fe_2O_3@HAp-CD and *d* CD

respectively. The resulted product was denoted as Fe_2O_3@HAp-NH_2.

2.2.2 Synthesis of Magnetite–Hydroxyapatite Anchored β-Cyclodextrin, γ-Fe_2O_3@HAp-CD

The 1,1-carbonyldiimidazole-β-cyclodextrin (CD-CDI) was synthesized according to previously reported method [61]. Briefly, β-cyclodextrin (0.42 g, 0.37 mmol) and 1,1-carbonyldiimidazole (0.49 g, 3 mmol) were dissolved in DMF (6 mL) and stirred with argon protection at room temperature for 2 h. The solution was then precipitated with cold diethyl ether and filtered. The resulting CD-CDI (0.45 g) dissolved in DMF (5 mL) and stored at 4 °C.

Fe_2O_3@HAp-NH_2 (1.0 g) nanocomposite was dispersed in DMF (50 mL) and stirred for 1.5 h. Next, CD-CDI was added into the dispersed solution of Fe_2O_3@HAp-NH_2. The mixture solution was further stirred in a three-neck flask with argon protection at room temperature for 7 h. The resulting precipitate was washed with DMF and acetone to remove unreacted chemicals. The precipitate, γ-Fe_2O_3@HAp-CD, was finally collected using a magnet and dried in a vacuum oven at 50 °C for 6 h.

2.2.3 Preparation of Ag Nanoparticles Incorporated Mesoporous Magnetite–Hydroxyapatite, γ-Fe_2O_3@HAp-CD.Ag

0.3 g of γ-Fe_2O_3@HAp-CD was dispersed in 100 mL freshly prepared an aqueous solution of $NaBH_4$ (0.003 M) and the mixture was stirred for 1 h in an ice bath. To the suspension, an aqueous solution of $AgNO_3$ (100 mL of 0.001 M) was added drop wise with constant stirring. After 2 h, the ice bath was removed and the suspension was stirred for 3 h. Finally, the nanocomposite, γ-Fe_2O_3@HAp-CD.Ag, was magnetically separated and washed with deionized water for several times and dried at 45 °C.

2.3 General Procedure for the Reduction of Nitro Compounds, Catalyzed by γ-Fe_2O_3@HAp-CD.Ag

To the suspension of nitro aromatic compound (1 mmol) in water (5 mL), $NaBH_4$ (5 mmol) and nanocomposite (0.05 g) were added and completely mixed at room temperature. The mixture was stirred at 80 °C for the time shown in Table 3. After completion of the reaction as indicated by TLC [using Et_2O/*n*-hexane as eluent: 1/5], the insoluble supported nanocatalyst was isolated with the aid of an external magnetic field and the aniline product was extracted from liquid with diethyl ether.

3 Results and Discussions

The synthetic route for the preparation of the Ag nanoparticles incorporated β-cyclodextrin conjugated magnetic hydroxyapatite, γ-Fe_2O_3@HAp-CD.Ag, is outlined in Scheme 1. As shown in Scheme 1, the organic–inorganic nanocomposite as prepared with a multistep process. Firstly, Fe_3O_4 nanoparticles was easily prepared by coprecipitation of ferrous and ferric ions in a basic aqueous solution followed by thermal treatment. Because of the sensitivity of the Fe_3O_4, its surface was coated with hydroxyapatite. The obtained, γ-Fe_2O_3@HAp powder was then conjugated with 3-aminopropyltrimethoxysilane to afford reactive amino groups. Subsequently, 1,1-carbonyldiimidazole-β-cyclodextrin (CD-CDI) was synthesized and grafted onto the surface of the γ-Fe_2O_3@HAp-NH_2. Finally, embedding of the silver nanoparticles into the nanocomposite, γ-Fe_2O_3@HAp-CD, was easily carried out by chemical reduction of

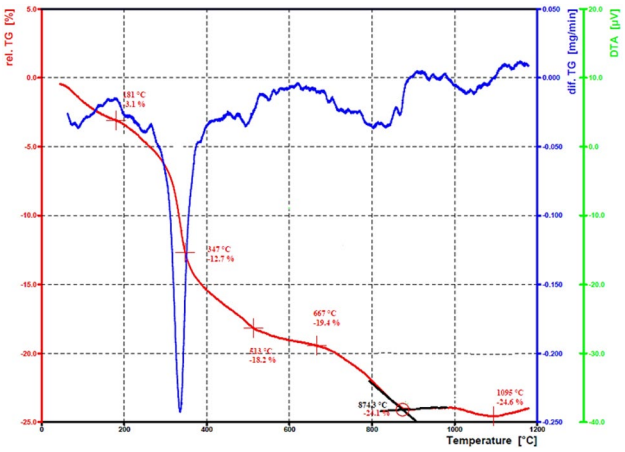

Fig. 2 TGA curve of γ-Fe_2O_3@HAp-CD.Ag

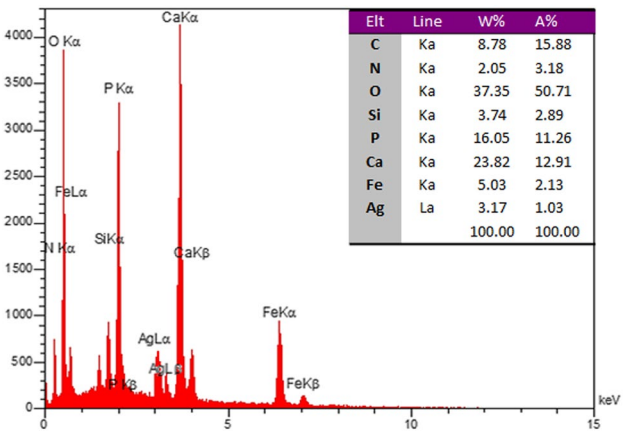

Fig. 3 EDS spectrum of γ-Fe_2O_3@HAp-CD.Ag

$AgNO_3$ by $NaBH_4$ in water and in the presence of γ-Fe_2O_3@HAp-CD.

The chemical structure of γ-Fe_2O_3@HAp-CD.Ag nonocatalyst was analyzed using FT-IR, TGA, EDS mapping, XRD, BET, FE-SEM, TEM and VSM analysis. To characterize the nanocomposite, and to confirm the immobilization of the active components on the pore surface of hydroxyapatite, FT-IR spectroscopy was initially utilized. Figure 1 shows the FT-IR spectra of the, γ-Fe_2O_3@HAp (a), γ-Fe_2O_3@HAp-NH_2 (b), γ-Fe_2O_3@HAp-CD (c), and β-CD (d) in the range of 400–4000 cm^{-1}. As shown in Fig. 1, characteristic absorption bands due to the bending vibration mode of O–P–O surface phosphate groups in the Hydroxyapatite were observed at 566 and 602 cm^{-1} which overlap with Fe–O bonds stretching, the adsorption band at 1034 cm^{-1} can be attributed to the stretching of the P–O bond (Fig. 1a–c). The peaks at 3571 and 632 cm^{-1} are due to OH^- ions. The broad bands in 3420 cm^{-1} and around 1639 cm^{-1} arise from water, the 1415 cm^{-1} peak is from CO_3^{2-} ions (Fig. 1a). For Fe_2O_3@HAp-NH_2 (Fig. 1b), peaks at 2928 and 1635 cm^{-1} were assigned to stretching vibration of C-H bonds of the aminopropyl groups and -NH stretching

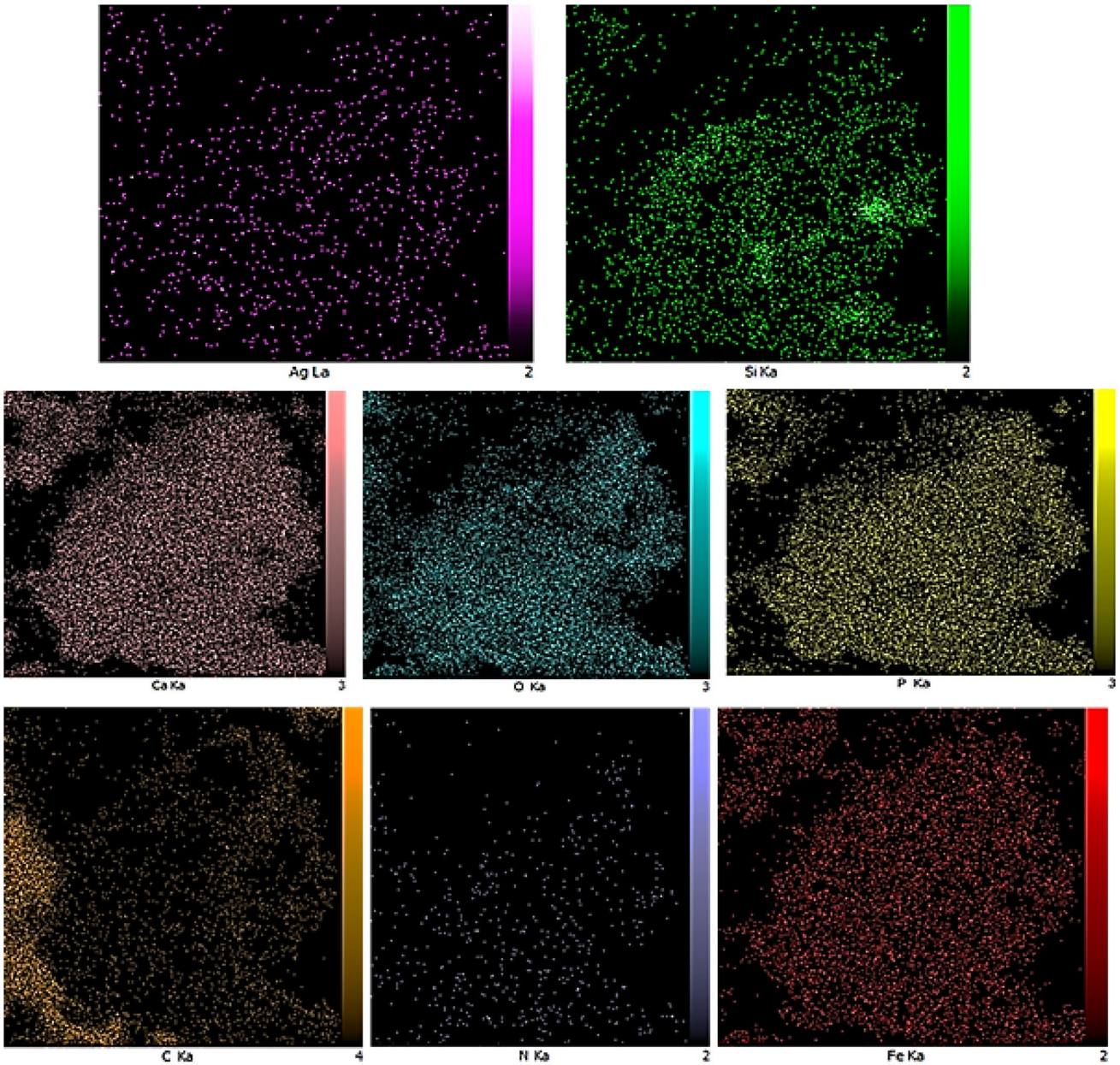

Fig. 4 EDS elemental mapping of the γ-Fe_2O_3@HAp-CD.Ag nanocatalyst

vibrations. The spectrum of β-CD (Fig. 1d) displayed characteristic peaks at 1650, 2928 and 1650 cm^{-1} were also observed in spectrum of Fe_2O_3@HAp-CD with little shift (Fig. 1c). The peak at 1744 cm^{-1} was assigned to carbonyl band in Fe_2O_3@HAp-CD, that show CD-CDI was covalently grafted onto the surface of Fe_2O_3@HAp-NH_2 (Fig. 1d). The result provides direct evidence that the conjugation occurs.

The stability of the nanocomposite was examined by Thermo-gravimetric analysis, TGA. As shown in Fig. 2, the first weight loss of 3.1% below 200 °C which might be due to the loss of the adsorbed water as well as dehydration of the surface OH groups. In the second region, the sharp decrease of weight in the range 300–700 °C is due to decomposition of CD and organic substances in Fe_2O_3@HAp-CD.Ag composite. After that, there was a weight loss from 800 °C to 1000 °C due to the decomposition of calcium carbonate to calcium oxide which verified the presence of hydroxyapatite. Thus, the TGA curves also confirm the successful grafting of β-cyclodextrin onto the magnetic surface of hydroxyapatite encapsulated -γ-Fe_2O_3.

Furthermore, the chemical composition of the γ-Fe_2O_3@HAp-CD.Ag nanocomposite was determined by energy dispersive X-ray spectroscopy (EDS). It is found that the peaks of C, N, O, Si, P, Ca, Fe and Ag are observed. The percentages of each element (of C, N, O, Si, P, Ca, Fe and Ag) of nanocatalyst are obtained from energy dispersive X-ray spectrum (Fig. 3). The presence and distribution of silver centers in the nanocomposite support, γ-Fe_2O_3@HAp-CD, is confirmed by elemental mapping images. The results show uniform distribution of silver nanoparticles over the structure of the hydroxyapatite support (Fig. 4). The incorporated Ag in the composite was also confirmed and determined by atomic absorption spectroscopy (AAS) (2 wt %).

Typical X-ray diffraction (XRD) patterns of the γ-Fe_2O_3@HAp-CD.Ag are shown in Fig. 5. The peaks at 2θ = 35.7°, 43.6°, 53.3°, 57.1° and 63.1° are attributed to γ-Fe_2O_3(marked ▼), in agreement with the standard reflection peaks (JCPOS card 25-1402), Hydroxyapatite also shows typical diffraction peaks, (marked O), at 2θ = 25.7°, 31.8°, 32.9°, 34.1°, 39.8°, 46.8°, and 49.4° (PDF-2-no. [084-1998] (ICDD)) [62]. In addition, the obvious diffraction peaks at 2θ values of 38.07°, 44.18°, 64.32° and 77.35° were corresponding to the (111), (200), (220) and (311) planes of silver, respectively. The size of the Ag nanoparticles is estimated 12 nm using the Scherrer's equation. This observation confirms the presence of silver particles in on the surface of nanocomposite.

Figure 6 represent the low temperature nitrogen adsorption–desorption isotherms and pore size distributions of γ-Fe_2O_3@HAp and γ-Fe_2O_3@HAp-CD.Ag samples which exhibit a type IV curve with a hysteresis loop. Type IV isotherms correspond to a mesoporous material. According to the report in Table 1 about Brunauer–Emmett–Teller (BET) surface area, pore volume and pore size of Fe_2O_3@HAp (BET: 143.97 $m^2\ g^{-1}$, pore volume: 0.57 $cm^3\ g^{-1}$ and pore size: 15.98 nm), decrease in these values is also possible proof that the organic groups and metal complex are successfully loaded onto the Fe_2O_3@HAp surface.

Figure 7 represents the results of field emission scanning electron micrograms (FESEM) in order to investigate the particle size, morphology and architecture of the γ-Fe_2O_3@HAp-CD.Ag nanocomposite. Also, FESEM images of the particles showed spherical

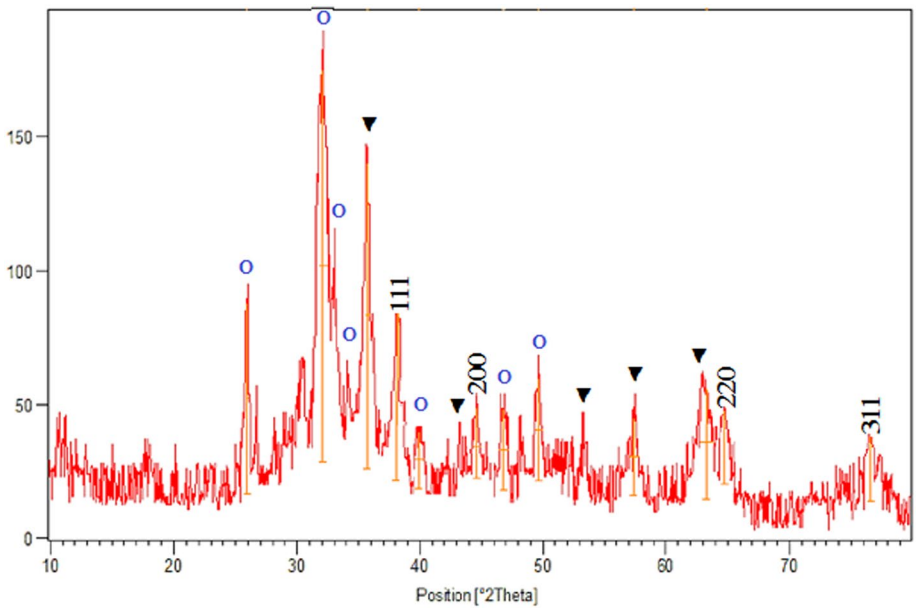

Fig. 5 XRD patterns of the γ-Fe_2O_3@HAp-CD.Ag nanocatalyst

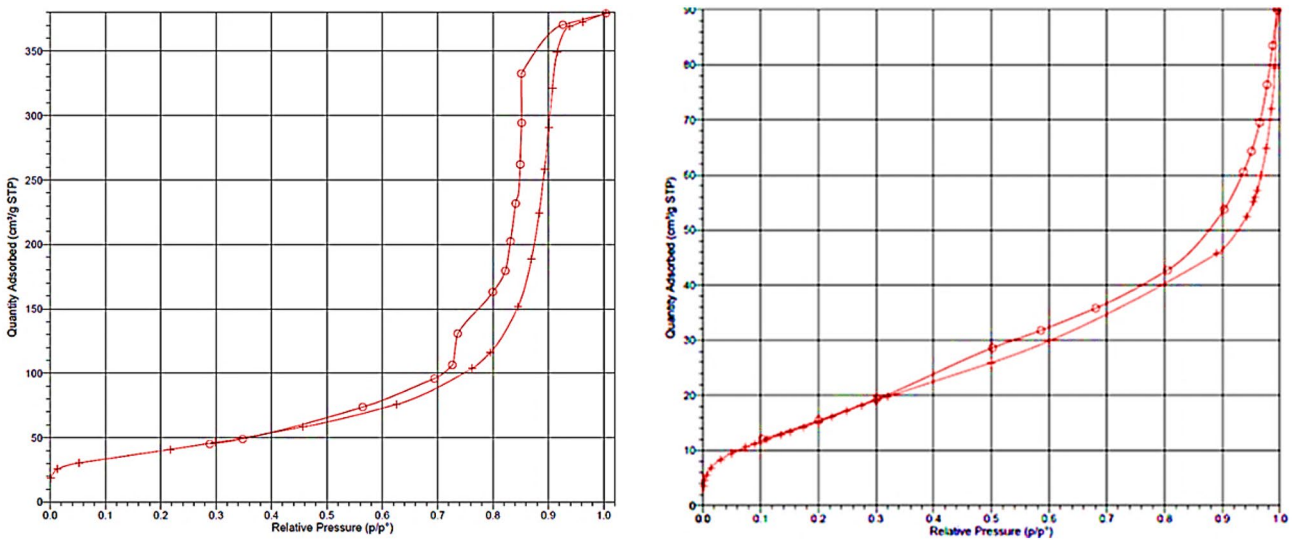

Fig. 6 Nitrogen adsorption/desorption isotherms curves of γ-Fe_2O_3@HAp (left) and γ-Fe_2O_3@HAp-CD-Ag (right)

Table 1 Comparison of the textural properties of γ-Fe_2O_3@HAp and γ-Fe_2O_3@HAp-CD.Ag

Samples	BET surface area ($m^2\ g^{-1}$)	Pore volume ($cm^3\ g^{-1}$)	Pore size (nm)
γ-Fe_2O_3@HAp	143.97	0.57	15.98
γ-Fe_2O_3@HAp-CD.Ag	58.20	0.08	5.25

shaped morphology and core–shell structured magnetic hydroxyapatite microspheres with nano dimension ranging under 30 nm (Fig. 7).

Transmission electron-microscopy (TEM) studies of the of γ-Fe_2O_3@HAp-CD.Ag organic–inorganic composites (Fig. 8) revealed that the Ag nanoparticles had been incorporated in the γ-Fe_2O_3@HAp-CD nanocomposite successfully. Some dark spots in the TEM images of γ-Fe_2O_3@HAp-CD.Ag can be attributed to the presence of silver nanoparticles in catalyst and the particles size of Ag (0) are around 13 nm which is nearly the value calculated from XRD data.

Magnetic properties of γ-Fe_2O_3@HAp, γ-Fe_2O_3@HAp-CD.Ag and Fe_3O_4 were investigated using a vibrating sample magnetometer (VSM) with a field of − 10,000 to 10,000 Oe at room temperature. As shown in Fig. 9, the M (H) hysteresis loop for the three samples was completely reversible, which indicated their superparamagnetic characteristics. The catalysts γ-Fe_2O_3@CD and γ-Fe_2O_3@HAp-CD.Ag demonstrated saturation magnetization values of 17.17 and 12.62 emu g^{-1}, respectively, while the Fe_3O_4 nanoparticle

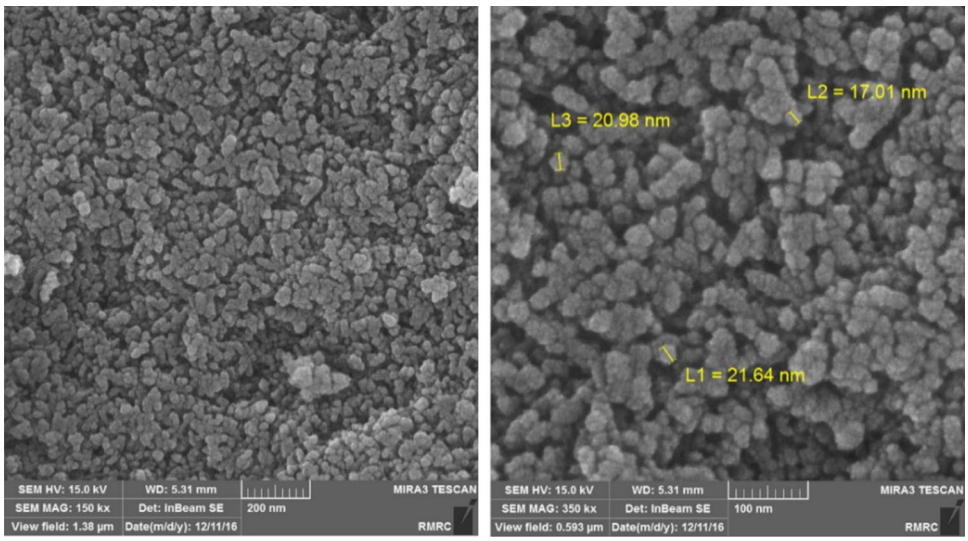

Fig. 7 FE-SEM image of γ-Fe_2O_3@HAp-CD.Ag

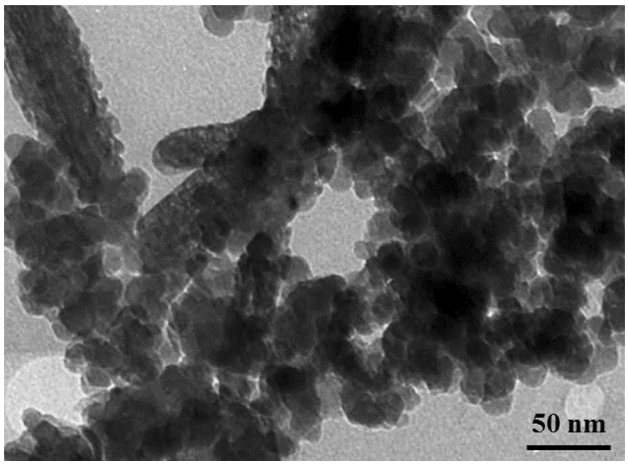

Fig. 8 TEM image of γ-Fe_2O_3@HAp-CD.Ag

had the value of 54.94 emu g^{-1}. The reason may be attributed to the grafting of β-CD and Ag, respectively, over γ-Fe_2O_3@HAp. However, the lower value of Fig. 9b, c is still enough to ensure the readily recovery of the catalysts from reaction mixture using external magnetic force.

The catalytic performance of the γ-Fe_2O_3@HAp-CD.Ag nanocomposite has been systematically studied in the aqueous reduction of nitroarenes by $NaBH_4$. The nitrobenzene reduction is commonly used as a model reaction to test the catalytic activity of various systems because of its significance. After some experiments, it was found that for facile reduction of 1 mmol of nitrobenzene, the use of 5 mmol of $NaBH_4$ in the presence of γ-Fe_2O_3@HAp-CD.Ag nanocomposite (0.05 g) at 80 °C in the water was the best condition. In order to elucidate the role of catalyst, a control reaction was set up in the absence of γ-Fe_2O_3@HAp-CD.Ag only

Table 2 Optimization of the amount of the γ-Fe_2O_3@HAp-CD.Ag as catalyst for the reduction of nitrobenzene in water at 80 °C

Entry	Catalyst (g)	$NaBH_4$ (mmol)	Time (min)	Yield (%)
1	–	5	300	Trace
2	0.03	5	45	90
3	0.05	5	30	98
4	0.05	6	30	98
5	0.08	5	25	98
6	0.1	5	25	98

trace amount of the desired product was observed on the TLC plate even after 5 h of heating. When the reaction was performed in the presence of the nanocatalyst, it proceeded rapidly to give the aniline (Table 2).

Using the optimized reaction conditions, the activity and synthetic scope of the catalyst was demonstrated by reduction of a series of nitroarenes (Table 3). As shown in Table 3, activated and deactivated groups have a very small authority on the reaction times and yields. In all cases, corresponding amines were found to be the exclusive product of the reactions according to TLC and the azo, hydrazo and azoxy groups as the usual side products in the reduction of nitroarenes were not detected.

A plausible reaction mechanism for the reduction of aromatic nitro compounds to corresponding amine using γ-Fe_2O_3@HAp-CD.Ag catalyst with $NaBH_4$ as hydrogen source showed in Scheme 2. The mechanism was proposed based on the reported literature [2]. The reduction of nitro compound involves electron transfer from $[BH_4]^-$ ion to the nitro compound through the γ-Fe_2O_3@HAp-CD.Ag catalyst. Thereby larger amount of hydride can be transferred or a

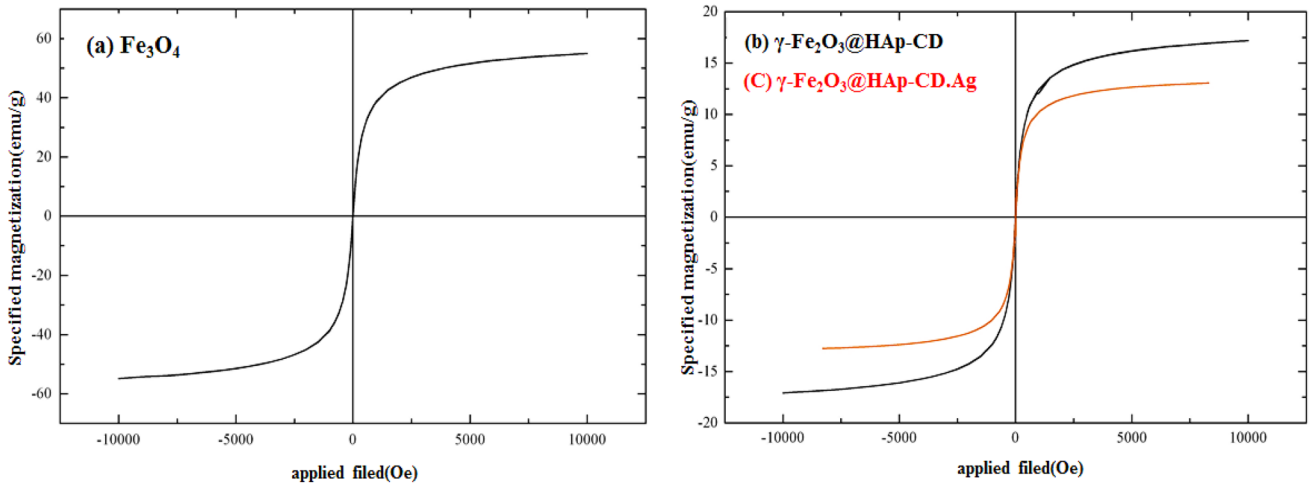

Fig. 9 Hysteresis loops of Fe_3O_4 (**a**), γ-Fe_2O_3@HAp-CD (**b**) and γ-Fe_2O_3@HAp-CD.Ag (**c**)

Table 3 Reduction of nitroarenes by $NaBH_4$ in the presence of γ-Fe_2O_3@HAp-CD.Ag in water ($NaBH_4$/nitro compound 5: 1, temperature 80 °C)

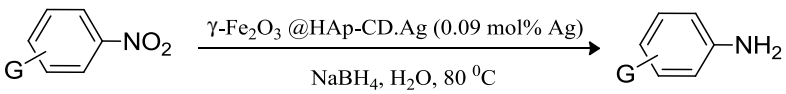

Entry	Nitro Compound	Product	Time (min)	Yield (%)
1	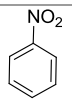	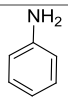	30	98
2	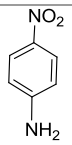	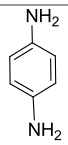	55	92
3	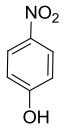	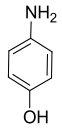	40	90
4	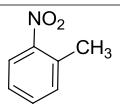	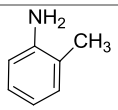	50	80
5	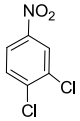	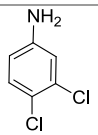	40	95
6	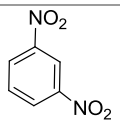	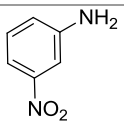	20	95
7	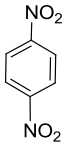	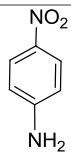	15	95
8	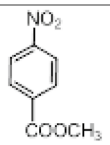	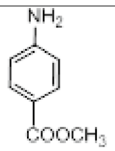	20	90
9	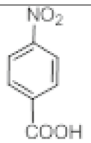	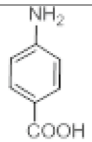	35	85

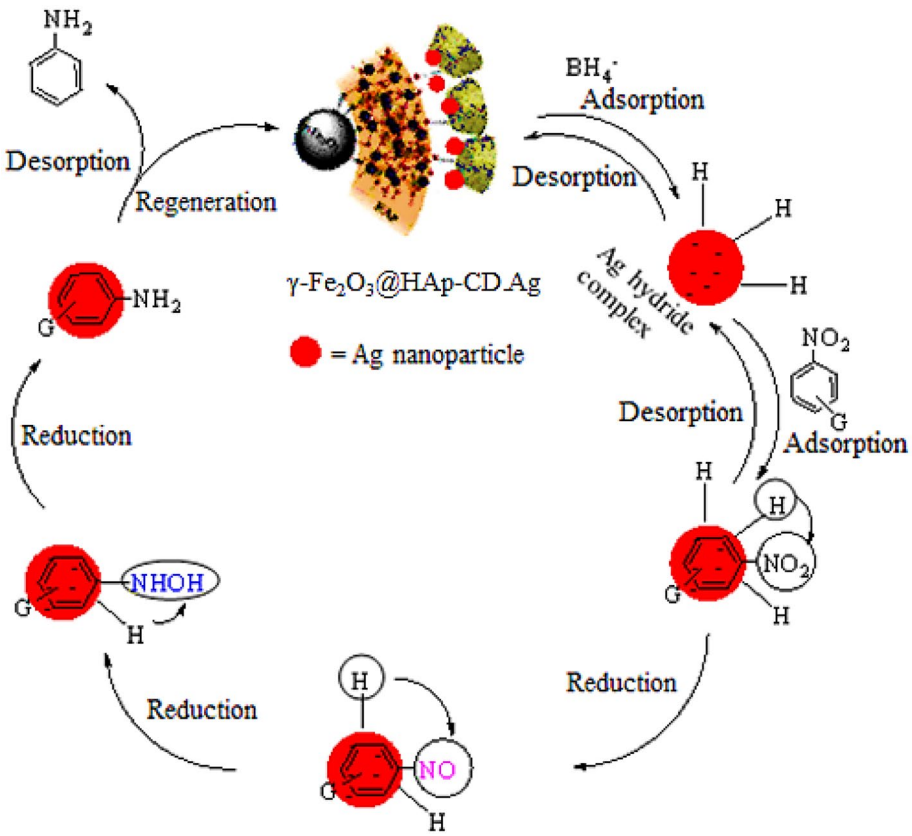

Scheme 2 A plausible reaction mechanism for the reduction of nitroarene using γ-Fe_2O_3@HAp-CD.Ag catalyst with $NaBH_4$ as hydrogen source

larger amount of H_2 gas can be produced in the reduction of nitro compound.

The durability of the catalyst was also tested. For this aim, after completion of the reduction of nitrobenzene, γ-Fe_2O_3@HAp-CD.Ag catalyst was easily separated from the reaction mixture by means of an external magnetic field. The catalytic performances of the γ-Fe_2O_3@HAp-CD.Ag used five different cycles under one constant set of operating conditions ($NaBH_4$/nitrobenzene: 5: 1, temperature: 80 °C, time: 30 min). The reduction rate decreased with increasing the run number (Fig. 10). These results confirmed that the reliability and practicality of this method. The reliability and practicality of this method were confirmed by these results.

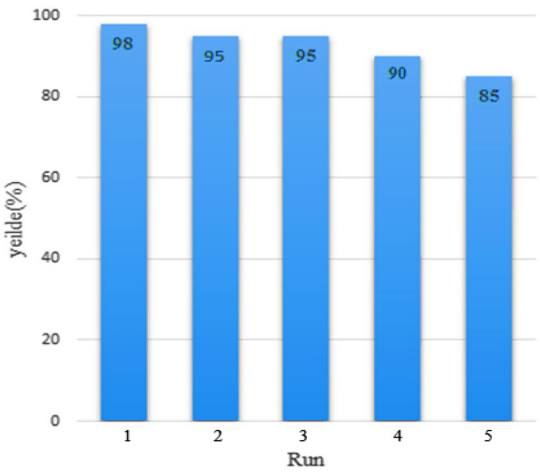

Fig. 10 Recyclability of γ-Fe_2O_3@HAp-CD.Ag in the nitrobenzene reduction

In view of the leaching problems observed with supported silver on γ-Fe_2O_3@HAp-CD.Ag, quantitative analysis using AAS was employed to determine the amount of metal in the reaction. The heterogeneity of the γ-Fe_2O_3@HAp-CD.Ag catalyst was examined by carrying out a hot filtration test using nitrobenzene as model substrates. No Silver could be detected in the liquid phase by AAS and more significantly, after hot filtration, the reaction of residual mixture was completely stopped.

To demonstrate the superiority of γ-Fe_2O_3@HAp-CD.Ag over the reported catalysts, the reduction of nitrobenzene was considered as a representative example (Table 4). While in all of these cases, comparative yields of the desired product were obtained following the γ-Fe_2O_3@HAp-CD.Ag catalyzed procedure. These results clearly demonstrate that the nanocomposite is an equally or more efficient catalyst for this reaction.

Table 4 A comparisons of the results of the present system with the some recently reported procedures

Entry	Catalytic system	Reaction conditions	Time (h)	Yield (%)	Ref.
1	Polymer supported palladium nanoparticles	$NaBH_4$, H_2O, R.T, catalyst (0.04 g)	6	96	[63]
2	NAP–Mg–Pd(0)/PS[a]	Et_3N, PMHS, H_2O, 80 °C, catalyst (0.02 g)	2	97	[64]
3	Silver nanoparticles immobilized to rice husk–SiO_2–aminopropylsilane composite	$NaBH_4$, H_2O, reflux, catalyst (0.5 g)	0.8	95	[65]
4	Scrap automobile catalyst	$NaBH_4$, EtOH/water (1/1), 5 °C, catalyst (0.3 g)	4	95	[66]
5	(c-Pt + Mo)/C[b]	EtOH/water, H_2 (4 bar, total pressure), 30 °C, catalyst (0.07 g)	0.8	99	[67]
6	Co catalyst	5.0 MPa H_2, 2 mL ethanol, 0.5 mL H_2O, 110 °C, 4.8 mol% catalyst (1.4 mg Co, 0.024 mmol, 35 mg)	15	> 99	[68]
7	Pd NPs/RGO	$NaBH_4$, EtOH:H_2O (v/v = 1:2), 50 °C, catalyst (6.0 mg)	1.5	98	[69]
8	Fe_3O_4@nSiO_2@mSiO_2/Pr-Imi-NH_2.Ag	$NaBH_4$, H_2O, 95 °C, catalyst (0.02)	0.75	98	[57]
9	AgNC	$NaBH_4$, RT, H_2O, catalyst (0.049 g, 5 mol%)	3.5	82	[70]
10	Fe@Ag-ATP-CA	$NaBH_4$(0.1 M), RT, H_2O, catalyst (1.4 g L^{-1})	–	–	[71]
11	γ-Fe_2O_3@HAp-CD.Ag	$NaBH_4$, H_2O, 80 °C, catalyst (0.05 g)	0.5	98	This work

[a]Polysiloxane-stabilised "Pd" nanoparticles on NAP–magnesium oxide supports

[b]Pt NPs supported on activated carbon and promoted by a molybdenum salt

4 Conclusion

In this study, we fabricated a novel nanocatalyst architecture of silver nanoparticles (0.09 mol% Ag) loaded into the β-cyclodextrin/γ-Fe_2O_3@ hydroxyapatite (γ-Fe_2O_3@HAp-CD.Ag) composite for the aqueous reduction of nitroarenes to the corresponding amines in good to excellent yields without affecting other vulnerable groups by using $NaBH_4$ as the source of hydrogen. Grafting of β-CD onto the magnetic nano-catalyst is confirmed by FT-IR, TGA, EDX mapping and XRD analyses The experimental results shown that surface of composite modified by β-CD can improve the catalytic performance of the silver nanoparticles Furthermore, the catalyst can be easily recovered from the reaction mixture by using a magnetic field and reused for five consecutive runs with a slight loss of catalytic activity. This novel methodology was also enhanced product purity and promises economic as well as environmental benefits.

Acknowledgements This work was supported by the Research Council at the Shahid Chamran University of Ahvaz.

References

1. Sharma RK, Dutta S, Sharma S, Zboril R, Varma VS, Gawande MB (2016) Green Chem 18:3184
2. Layek K, Kantam ML, Shirai M, Nishio-hamane D, Sasaki T, Maheswaran H(2012) Green Chem 14:3164
3. Jain AK, Gupta VK, Bhatnagar A (2003) Sep Sci Technol 38:463
4. Gupta VK, Kumar R, Nayak A, Saleh TA, Barakat MA (2013) Adv Colloid Interface Sci 193:24
5. Khani H, Rofouei MK, Arab P, Gupta VK, Vafaei Z (2010)) J Hazard Mater 183:402
6. Gupta VK, Saleh TA (2013) Environ Sci Pollut Res 20:2828
7. Gupta VK, Ali I, Saleh TA, Nayak A, Agarwal S (2012) RSC Adv 2:6380
8. Igder S, Kiasat AR, Shushizadeh MR (2015) Res Chem Intermed 41:7227
9. Mouradzadegun A, Ma'mani L, Mahdavi M, Rashid Z, Foroumadi A, Dianat S(2015) RSC Adv 4:116
10. Jiang L, Li Y, Xiong C, Su S(2017) Mater Sci Eng C 75:1014
11. Zarei Z, Akhlaghinia B(2016) RSC Adv 6:106473
12. Zhang Z, Yuan Z, Tang D, Ren Y, Lv K, Liu B(2014) ChemSusChem 7:3496
13. Ramos Guivar JA, Sanches EA, Bruns F, Sadrollahi E, Morales MA, López EO, Litterst FJ (2016) Appl Surf Sci 389:721
14. Begum R, Farooqi ZH, Ahmed E, Naseem K, Ashraf S, Sharif A, Rehan R (2017) Appl Organomet Chem 31. https://doi.org/10.1002/aoc.3563
15. Scialla S, Palazzo B, Barca A, Fiore A, Monteduro AG, Sannino A, Gervaso F, Maruccio G(2017) Mater Sci Eng C 76:1166
16. Tang W, Zhao J, Sha B, Liu H (2013) J Appl Polym Sci 127:2803
17. Ramimoghadam D, Bagheri S, Abd Hamid SB (2015) Colloids Surf B 133:388
18. Monteiro AP, Caminhas LD, Ardisson JD, Paniago R, Cortés ME, Sinisterra RD(2017) Carbohydr Polym 163:1
19. Son KD, Kim Y (2013) Mater Sci Eng C 33:499
20. Xiao X, Liu R, Qiu C, Zhu D, Liu F (2009) Mater Sci Eng C 29:785
21. Ai M, Du Z, Zhu S, Geng H, Zhang X (2017) Dent Mater 33:12
22. Dindulkar SD, Jeong D, Kim H, Jung S(2016) Carbohydr Res 430:85
23. Shao K, Zhang C, Ye S, Cai K, Wu L, Wang B, Zou C, Lu Z, Han H (2017) Sensors Actuators B 240:586
24. Li P, Li S, Wang Y, Zhang Y, Han G (2017) Colloids Surf A 520:26
25. Luo G, Kang L, Zhu M, Dai B (2014) Fuel Process Technol 118:20
26. Lu AS, Yu J, Cheng Y, Barras A, Xu W, Szunerits S, Cornu D, Boukherroub R (2017) Appl Surf Sci 411:163
27. Saravanan R, Gupta VK, Mosquera E, Gracia F (2014) J Mol Liq 198:409
28. Saravanan R, Prakash T, Gupta VK, Stephen A (2014) J Mol Liq 193:160

29. Saravanan R, Karthikeyan N, Gupta VK, Thirumal E, Thangadurai P, Narayanan V, Stephen A (2013) Mater Sci Eng C 33:2235
30. Saravanan R, Gupta VK, Narayanan V, Stephen A (2013) J Mol Liq 181:133
31. Gupta VK, Nayak A (2012) Chem Eng J 180:81
32. Saleh TA, Gupta VK (2012) J Colloid Interface Sci 371:101
33. Saravanan R, Sacari E, Gracia F, Khan MM, Mosquera E, Gupta VK (2016) J Mol Liq 221:1029
34. Devaraj M, Saravanan R, Deivasigamani R, Gupta VK, Gracia F, Jayadevan S (2016) J Mol Liq 221:930
35. Rajendran S, Khan MM, Gracia F, Qin J, Gupta VK, Arumainathan S (2016) Sci Rep 6:31641
36. Saleh TA, Gupta VK (2011) J Colloid Interface Sci 362:337
37. Ahmaruzzaman M, Gupta VK (2011) Ind Eng Chem Res 50:13589
38. Mohammadi N, Khani H, Gupta VK, Amereh E, Agarwal S (2011) J Colloid Interface Sci 362:457
39. Saleh TA, Gupta VK (2012) Sep Purif Technol 89:245
40. Saleh TA, Gupta VK (2012) Environ Sci Pollut Res 19:1224
41. Saravanan R, Gracia F, Khan MM, Poornima V, Gupta VK, Narayanan V, Stephen A (2015) J Mol Liq 209:374
42. Russo M, Armetta F, Riela S, Martino DC, LoMeo P, Noto R (2015) J Mol Catal A 408:250
43. Dong Z, Le X, Li X, Zhang W, Dong C, Ma J (2014) Appl Catal B 158:129
44. Chi Y, Tu J, Wang M, Li X, Zhao Z (2014) J Colloid Interface Sci 423:54
45. Sharma M, Sarma PJ, Goswami M, Bania KK (2017) J Colloid Interface Sci 490:529
46. Wang H, Wang H, Li T, Ma J, Li K, Zuo X (2017) Sensors Actuators B 239:1205
47. Wang M, Wang J, Wang Y, Liu C, Liu J, Qiu Z, Xu Y, Lincoln SF, Guo X (2016) Colloid Polym Sci 294:1087
48. Saravanan R, Joicy S, Gupta VK, Narayanan V, Stephen A (2013) Mater Sci Eng C 33:4725
49. Saravanan R, Karthikeyan S, Gupta VK, Sekaran G, Narayanan V, Stephen A (2013) Mater Sci Eng C 33:91
50. Saravanan R, Thirumal E, Gupta VK, Narayanan V, Stephen A (2013) J Mol Liq 177:394
51. Saravanan R, Gupta VK, Prakash T, Narayanan V, Stephen A (2013) J Mol Liq 178:88
52. Gupta VK, Jain R, Mittal A, Saleh TA, Nayak A, Agarwal S, Sikarwar S (2012) Mater Sci Eng C 32:12
53. Karthikeyan S, Gupta VK, Boopathy R, Titus A, Sekaran G (2012) J Mol Liq 173:153
54. Saravanan R, Gupta VK, Narayanan V, Stephen A (2014) J Taiwan Inst Chem Eng 45:1910
55. Shiraishi Y, Kanzaki T, Sawai H, Asano H, Du Y, Toshima N (2016) Bull Soc Photogr Image Jpn 26:14
56. Liang Y, Lin C, Guan J, Li Y (2017) RSC Adv 7:7460
57. Nasab MJ, Kiasat AR (2016) RSC Adv 6:41871
58. Saravanan R, Gupta VK, Mosquera E, Gracia F, Narayanan V, Stephen A (2015) J Saudi Chem Soc 19:521
59. Saravanan R, Khan MM, Gupta VK, Mosquera E, Gracia F, Narayanan V, Stephen A (2015) RSC Adv 5:34645
60. Saravanan R, Khan MM, Gupta VK, Mosquera E, Gracia F, Narayanan V, Stephen A (2015) J Colloid Interface Sci 452:126
61. Cai K, Li J, Luo Z, Hu Y, Hou Y, Ding X (2011) Chem Commun 47:7719
62. Zhang Z, Zhen J, Liu B, Lv K, Deng K (2015) Green Chem 17:1308
63. Dell'Anna MM, Intini S, Romanazzi G, Rizzuti A, Leonelli C, Piccinni F, Mastrorilli P (2014) J Mol Catal A 395:307
64. Online VA, Damodara D, Arundhathi R, Babu TVR, Legan MK, Kumpaty HJ, Likhar PR (2014) RSC Adv 43:22567
65. Davarpanah J, Kiasat AR (2013) Catal Commun 41:6
66. Genc H (2015) Catal Commun 67:64
67. Boymans E, Boland S, Witte PT, Müller C, Vogt D (2013) ChemCatChem 5:431
68. Schwob T, Kempe R (2016) Angew Chem Int Ed 48:15175
69. Nasrollahzadeh M, Sajadi SM, Rostami-vartooni A, Alizadeh M, Bagherzadeh M (2016) J Colloid Interface Sci 466:360
70. Giri S, Das R, Van Der Westhuyzen C, Maity A (2017) Appl Catal B. https://doi.org/10.1016/j.apcatb.2017.03.033
71. Gupt VK, Yola ML, Eren T, Kartal F, Çağlayan MO, Atar N (2014) J Mol Liq 190:133

Affiliations

Maedeh Azaroon[1] · Ali Reza Kiasat[1,2]

[1] Chemistry Department, College of Science, Shahid Chamran University of Ahvaz, Ahvaz, Iran

[2] Petroleum Geology and Geochemistry Research Centre (PGGRC), Shahid Chamran University of Ahvaz, Ahvaz, Iran